

31 the outer tubes, to take due account of outward-only local buckling, and the effective
32 compressive strength of the infilled concrete, to reflect the reduced relative effectiveness of
33 higher concrete grades, are considered. The modified design rules are shown to improve the
34 accuracy and consistency of the design capacity predictions. Finally, statistical analyses were
35 carried out to demonstrate the reliability of the modified design approaches.

36

37 **1. Introduction**

38 The use of concrete-filled steel tubular (CFST) cross-sections for compression members has
39 become increasingly widespread in construction, owing primarily to their superior strengths,
40 stiffnesses and ductility over plain concrete or hollow steel tubes [1,2]. The interaction between
41 the concrete infill and the outer metal tube leads to efficient utilisation of both constituent
42 materials by confining the concrete core and delaying local buckling of the metal tube, thereby
43 improving the cost-effectiveness of the system. Recently, research efforts have turned towards
44 concrete-filled double skin tubular (CFDST) cross-sections, comprising two metal tubes and
45 sandwiched concrete-filled between the tubes [3-7]. CFDST cross-sections share most of the
46 benefits of CFST cross-sections, but will typically be lighter owing to the absence of the inner
47 concrete core. This facilitates assembly and deconstruction and reduces foundation costs,
48 making CFDST cross-sections an attractive choice for heavy structural applications. Such
49 potential applications include offshore structures [3] and bridge piers [4]; an early example of
50 the use of CFDST columns in a transmission tower is described in [5].

51

52 Stainless steel members possess a unique combination of excellent mechanical properties for
53 structural applications and corrosion resistance, and have been utilised in construction
54 increasingly over the past few decades [8]. An innovative form of CFDST cross-section,
55 utilising stainless steel for the outer tube, was recently proposed [9–12], with the aim of

56 exploiting the most favourable properties of the constituent materials to the greatest possible
57 extent. CFDST columns using stainless steel for the outer tubes were found to exhibit a rather
58 more rounded and ductile load-deformation response compared to their carbon steel
59 counterparts [10–12]. These observations mirror the findings for concrete-filled stainless steel
60 tubular stub columns in a number of recent studies, including concrete-filled stainless steel stub
61 columns with circular [13], rectangular [14–16] and square [14–17] cross-sections. This
62 behaviour is directly linked to the rounded stress–strain response and substantial strain
63 hardening that characterises stainless steel alloys. The combined advantages of the composite
64 action seen in CFDST member, alongside and the durability and ductility associated with
65 stainless steel, make this section type potentially suitable for applications in demanding and
66 aggressive environments, such as in offshore and marine structures, bridges and the nuclear
67 industry.

68
69 Research into CFDST members dates back about 20 years and has mainly focussed on CFDST
70 sections employing carbon steel tubes and sandwiched concrete grades up to 72 MPa [18].
71 CFDST sections with stainless steel outer tubes have been the subject of only a few studies,
72 where their structural performance has been examined through experimentation and numerical
73 analysis. Han et al. [9] carried out a preliminary experimental investigation to examine the
74 behaviour of CFDST stub columns with austenitic stainless steel outer tubes. Further tests were
75 conducted by the authors of the present paper [10] to examine the cross-sectional behaviour and
76 resistances of CFDST stub columns with lean duplex and ferritic stainless steel outer tubes in
77 pure compression. Meanwhile, the authors [11,12] also examined CFDST stub columns
78 comprising austenitic stainless steel outer tubes and high strength steel inner tubes
79 experimentally and numerically. FE analyses were employed by Hassanein and Kharoob [19]
80 and Wang et al. [20] with the focus on CFDST cross-sections with circular hollow section (CHS)

81 inner tubes. To date, investigations into the structural performance of CFDST members
82 employing stainless steel as the outer tubes have been rather limited, and the design of these
83 members is not explicitly covered by current codes of practice. This prompted a thorough
84 programme of research performed by the authors, aimed at examining the behaviour and
85 capacity of CFDST structural members with stainless steel outer tubes of varying cross-section
86 shape and devising efficient structural design rules to support their application in practice. The
87 present paper focuses on the compressive behaviour and design of CFDST cross-sections with
88 square or rectangular hollow section (SHS/RHS) lean duplex or ferritic stainless steel outer
89 tubes and SHS carbon steel inner tubes.

90

91 A finite element (FE) investigation into the compressive behaviour of the examined CFDST
92 cross-sections is reported. The numerical modelling programme comprises a validation study
93 to replicate the structural response observed in available experiments described in the literature,
94 and a parametric study to generate further FE data on CFDST sections of varying local
95 slendernesses and material strengths. Based on the generated FE results, the influence of the
96 local slendernesses of the outer and inner tubes, the concrete strength and the grade of stainless
97 steel, on the ultimate response of the studied CFDST sections in compression is examined. The
98 combined set of FE and test data is then adopted to assess the applicability of current design
99 rules for concrete-filled members set out in the European Code EN 1994-1-1 (EC4) [21],
100 Australian Standard AS5100 [22] and American Specifications AISC 360 [23] and ACI 318
101 [24] to the design of the studied CFDST cross-sections. Modifications to the design treatment
102 in relation to the effective areas of the outer tubes and the effective compressive strength of the
103 concrete are considered. Finally, the reliability of the modified design approaches is evaluated
104 through statistical analyses.

105

106 **2. Review of existing experimental data**

107 A number of experimental investigation into the compressive behaviour of CFDST cross-
108 sections with stainless steel outer tubes have been carried out [9–12], but the only previous
109 experiments on CFDST cross-sections with SHS carbon steel inner tubes and SHS/RHS lean
110 duplex and ferritic stainless steel outer tubes (see Fig. 1), which are the focus of the present
111 study, were reported in Wang et al. [10]. In the study of Wang et al. [10], stub column tests
112 were conducted on eight different cross-sections with lean duplex stainless steel (Grade 1.4062)
113 RHS 150×80×3 (depth × width × thickness in mm) and SHS 100×100×3 or ferritic stainless
114 steel (Grade 1.4003) RHS 120×80×3 and 100×80×4 as the outer tubes, and carbon steel (Grade
115 S275) SHS 20×20×2.5, 20×20×1.5, 40×40×4 and 40×40×1.5 as the inner tubes. For each cross-
116 section, three concrete grades with nominal concrete cylinder compressive strengths of 40, 80
117 and 120 MPa were employed. A total of 28 stub column tests was carried out employing the
118 experimental rig shown in Fig. 2(a); a full description of the stub column tests is provided in
119 Wang et al. [10]. The observed failure modes featured outward-only local buckling of the
120 stainless steel outer tubes, crushing of the infill concrete, as well as local buckling of the carbon
121 steel inner tube, as displayed in Fig. 3. A summary of the measured geometric and material
122 properties, as well as the obtained experimental failure load for each stub column specimen is
123 reported in Table 1, where D_o/t_o and D_i/t_i are the overall depth-to-thickness ratios of the outer
124 and inner tubes respectively, in which D_o and D_i correspond to the overall depths of the outer
125 and inner tubes, t_o and t_i are the corresponding thicknesses, $\sigma_{0.2,o}$ and $\sigma_{0.2,i}$ correspond to the
126 material 0.2% proof stresses of the outer and inner tubes, f_c is the cylinder compressive strength
127 of the concrete and N_{exp} is the experimental failure load.

128

129 **3. Numerical modelling programme**

130 A comprehensive numerical modelling programme was performed employing the general-
131 purpose finite element (FE) analysis package ABAQUS [25]. FE models were established with
132 the aim of (i) replicating the compressive behaviour of the CFDST stub column test specimens
133 reported in [10] and (ii) performing a parametric study to derive further FE data and investigate
134 the influence of key variables on the structural performance of the studied CFDST cross-
135 sections in compression. The main features of the FE models are described in Section 3.1, while
136 the validation and parametric studies are reported in Sections 3.2 and 3.3, respectively.

137

138 **3.1 Development of finite element models**

139 ***3.1.1. Element types and discretisation***

140 FE models of all test specimens presented in Section 2 were established employing C3D8R [25]
141 solid elements for the concrete and S4R [25] shell elements for the metal tubes, in line with
142 previous numerical modelling of concrete-filled tubular members [11,12,26–29]. A systematic
143 mesh sensitivity study was undertaken to decide upon suitable mesh settings for the FE models,
144 in order to produce accurate yet computationally efficient results. For the cold-formed metal
145 tubes, the element size for the flat portions was chosen to be equal to the respective cross-
146 section thickness, while each corner of the cross-section was uniformly discretised into at least
147 four elements to ensure a precise representation of the curved corner geometry. For the
148 sandwiched concrete, the element sizes were selected to match those of the adjacent metal tubes
149 in order to facilitate numerical convergence.

150

151 ***3.1.2. Material Modelling***

152 The material constitutive properties of the metal tubes were represented by multi-linear elastic-
153 plastic stress–strain curves with isotropic hardening in ABAQUS [25]. The input true stress–
154 true plastic strain data set was derived from the measured engineering stress–strain curves,

155 characterised by at least 100 intervals to ensure the full range of the response was accurately
156 captured. The cold-formed metal tubes experienced plastic deformations during the cold-rolling
157 process, causing an increase in strength and a loss in ductility. This is particularly pronounced
158 in the corner regions and more significant in stainless steel, as observed from the coupon test
159 results reported by Wang et al. [10]. The yield strengths of the corner materials were found to
160 be about 50%, 35% and 10% higher, on average, than those of the flat materials for the lean
161 duplex stainless steel, ferritic stainless steel, and carbon steel sections, respectively. Hence,
162 allowance for this was made in the current FE models by assigning the corner material
163 properties to the respective curved corner regions and the adjacent flat regions beyond the
164 corners by a distance of two times the cross-section thickness, following the recommendations
165 of [30].

166

167 The material properties of the sandwiched concrete were characterised by the built-in concrete
168 damage plasticity (CDP) model in ABAQUS [25]. The Poisson's ratio of the concrete and
169 modulus of elasticity E_c were set respectively equal to 0.2 and $4733\sqrt{f_c}$, respectively, in
170 accordance with ACI 318 [24]. For the compressive properties of the concrete used in the CDP
171 model, a confined concrete stress–strain curve was adopted to take due account of the
172 confinement afforded to the concrete by the metal tubes. The confined stress–strain curve was
173 originally calibrated against test data on carbon steel CFST stub columns with concrete cylinder
174 compressive strengths ranging from 13 to 164 MPa by Tao et al. [28], and modified by the
175 authors [11,12] for application to CFDST stub columns with stainless steel outer tubes. The
176 modifications were concerned primarily with the confinement factor (ξ_c), as defined by Eq. (1),

177

$$\xi_c = \frac{A_o \sigma_{0.2,o}}{A_{ce} f_c} \quad (1)$$

178 where A_o is the cross-sectional area of the outer tube and A_{ce} is an equivalent cross-sectional
179 area of the sandwiched concrete, defined as the full area enclosed by the outer tube, as given
180 by Eq. (2), where $r_{int,o}$ is the internal corner radius of the outer tube.

$$181 \quad A_{ce} = (D_o - 2t_o)^2 - (4 - \pi)r_{int,o}^2 \quad (2)$$

182 For the tensile properties of the concrete used in the CDP model, a stress–strain curve
183 comprising a linear response up to the ultimate tensile strength, taken as $0.1f_c$, and a descending
184 branch characterised by fracture energy (G_F) [25,28], was adopted throughout the numerical
185 modelling programme.

186

187 ***3.1.3. Boundary conditions and interactions***

188 The geometry, loading and experimentally observed failure modes of the studied CFDST
189 specimens were doubly symmetric. Hence, to enhance computational efficiency, only one-
190 quarter of the cross-sections and half of the stub column lengths were modelled, with suitable
191 boundary conditions assigned to the planes of symmetry, as depicted in Fig. 2(b). For ease of
192 application of boundary conditions, the end sections of the three constituent parts of the CFDST
193 stub columns were coupled to three reference points, which were restrained against all degrees
194 of freedom except longitudinal translation in order to attain fixed-ended boundary conditions.
195 The same value of longitudinal displacement was applied at the three reference points to mimic
196 the displacement-controlled compressive loading scheme used in the experiments.

197

198 The interaction between the outer and inner tubes and the concrete was modelled using surface-
199 to-surface contact. “Hard contact” was employed in the normal direction, while the Coulomb
200 friction model was adopted to simulate the tangential behaviour. A value of 0.6 was selected
201 for the friction coefficient, though a prior sensitivity study had revealed that the compressive
202 response of the studied CFDST cross-sections was relatively insensitive to variation in this

203 parameter [31]. This is primarily due to the nature of the loading (i.e. axial compression), under
204 which the slip at the interfaces was negligible since the concrete and the metal tubes largely
205 deform together.

206

207 ***3.1.4. Initial imperfections and residual stresses***

208

209 Local geometric imperfections and residual stresses have negligible influence on the behaviour
210 of CFDST stub columns, owing principally to the fact that (i) the lateral pressure applied to the
211 steel tubes from the expansion of the concrete obviates the need to assign any geometric
212 perturbation to induce local buckling, and (ii) the support afforded to the metal tubes by the
213 concrete lessens the sensitivity of the tubes to local instabilities [11,12]. Therefore, local
214 geometric imperfections and residual stresses were not explicitly included in the current FE
215 models. The suitability of this treatment is confirmed through the validation of the FE models
216 reported in Section 3.2.

217

218 ***3.1.5. Solution schemes***

219 The modified Riks method (Riks) is commonly adopted for solving static numerical problems
220 with geometrical and material nonlinearities [25], and was generally employed in the present
221 study for the displacement-controlled nonlinear numerical analyses of the CFDST stub columns.
222 However, for some of the models, particularly those with more slender metal tubes,
223 convergence problems inhibited attainment of the peak loads or tracing of the post-ultimate
224 responses. In these cases, an adaptive automatic stabilisation scheme [25], which allows the
225 model to be stabilised by implementing an artificial viscous damping force, was employed in
226 the FE simulations. This approach has been successfully utilised for cold-formed steel members
227 and systems in [32,33], and shown to achieve satisfactory results provided that a sufficient

228 number of increments are achieved before the peak load is reached and that the ratio of the
229 energy dissipated by viscous damping (ALLSD) to the total strain energy (ALLIE) remains low.
230 In this study, at least 50 successful increments prior to reaching the peak load were achieved
231 and the ratios of ALLSD/ALLIE remained below 2%. The load versus average axial strain
232 (defined as the axial shortening divided by the stub column length) curve obtained using the
233 automatic stabilisation scheme is compared with that obtained using the modified Riks method
234 in Fig. 4 for a typical FE model featuring an SHS 600×600×12 lean duplex outer tube, an SHS
235 300×300×5 carbon steel inner tube and a concrete strength of 40 MPa; this specimen is denoted
236 LS600×12-NS300×5-C40 herein. The comparison reveals that similar results are achieved
237 using the two solution schemes with a maximum discrepancy of approximately 1% at the peak
238 load.

239

240 **3.2. Validation of FE model**

241 The developed FE model was validated with reference to the results of the tested CFDST stub
242 columns presented in Section 2; comparisons were made of the ultimate loads, load–
243 displacement curves and failure modes. Table 1 reports the numerical to experimental ultimate
244 compressive capacity ratio (N_{FE}/N_{exp}) for each tested CFDST specimen. A mean value of
245 N_{FE}/N_{exp} of 1.02 with a coefficient of variation (COV) of 0.035 was achieved, indicating that
246 the FE ultimate strengths are in close agreement with those obtained from the tests. The FE
247 models were also found to reproduce accurately the full load–deformation histories of the
248 respective stub column tests, examples of which are displayed in Fig. 5. The exhibited failure
249 modes were also well replicated numerically, as shown in Fig. 3. Overall, it may be concluded
250 that the established FE models can accurately and reliably simulate the experimental structural
251 responses of the examined CFDST stub columns.

252

253 3.3. Parametric study

254 The successfully validated FE models were utilised to acquire further FE data on CFDST cross-
255 sections with varying cross-section slendernesses and material strengths. The CFDST cross-
256 sections included in the parametric study cover compact, noncompact and slender cross-
257 sections, with reference to the classification limits for composite cross-sections in AISC 360
258 [23]. Regarding the geometric properties of the modelled cross-sections, the inner and outer
259 tubes were SHS with overall widths fixed at 300 and 600 mm, respectively, while the
260 thicknesses were varied to generate a wide spectrum of local slenderness values (d_i/t_i and d_o/t_o)
261 from 6 to 146, where d_i and d_o are the flat element widths of the inner and outer tubes. Note
262 that the studied d_o/t_o ratios cover the practical range of available rolled stainless steel sections
263 but also extend to more slender sections, which could be produced by press-braking, to assess
264 their performance in concrete-filled tubular construction. The internal corner radii of the outer
265 and inner tubes were set equal to the respective section thicknesses. The length of each FE
266 model was equal to $2.5D_o$, mirroring the test specimens. Throughout the parametric study, the
267 measured material properties of the tested lean duplex stainless steel SHS 100×100×3 and
268 ferritic stainless steel RHS 120×80×3 were used for the outer tubes, while those of the tested
269 carbon steel SHS 40×40×4 were used for the inner tubes. Three concrete grades with concrete
270 compressive strengths of 40, 80 and 120 MPa were adopted. Table 2 lists the ranges of variation
271 of the aforementioned parameters considered herein. Overall, a total of 311 CFDST specimens
272 was simulated in the parametric study.

273

274 The derived FE results were employed to examine the influence of the key variables on the
275 ultimate strength of the studied CFDST stub columns (N_u), including the local slendernesses of
276 the outer and inner tubes, the concrete grade and the stainless steel grade. Note that the load–
277 axial strain curves for some compact specimens did not reach their peak loads despite large

278 plastic deformations. For these specimens, the ultimate strength was defined as the load at
279 which the tangent stiffness of the load–axial strain curve at increment i , K_i , reached 1% of its
280 initial stiffness, K_{ini} — i.e. failure was taken at the point when $K_i/K_{ini} = 0.01$, a typical example
281 of which is illustrated in Fig. 6. This approach was proposed by dos Santos et al. [34] and has
282 been employed for the definition of the ultimate strengths of concrete-filled tubular members
283 in [11,12,14].

284

285 **3.3.1 Influence of local slenderness of metal tube**

286 The influence of the local slenderness of the outer tube on the ultimate response is assessed
287 through comparisons among specimens with the same inner tubes and concrete grades but
288 varying local slenderness values for the outer tube (d_o/t_o). In the comparisons presented, the
289 ultimate strength (N_u) obtained from the CFDST stub column FE simulations are normalised
290 by the respective plastic strength (N_{pl}) of the cross-sections, as defined by Eq. (3), which is a
291 simple summation of the plastic resistances of the outer tube, concrete and inner tube.

$$292 \quad N_{pl} = A_o \sigma_{0.2,o} + A_c f_c + A_i \sigma_{0.2,i} \quad (3)$$

293

294 The results are displayed in Fig. 7, where the normalised strength (N_u/N_{pl}) is plotted against the
295 local slenderness of the outer tube d_o/t_o . A total of 10 groups of data, differentiated by the local
296 slenderness of inner tube d_i/t_i , are compared, each comprising a spectrum of d_o/t_o ratios ranging
297 from 4 to 146. It can be observed that the specimens with the more compact outer tubes
298 exhibited the higher values of N_u/N_{pl} ; this is attributed to the reduced susceptibility to local
299 buckling and the improved confinement afforded to the concrete. Typical load–axial strain
300 curves, shown for specimens LS600×5-NS300×10-C40, LS600×20-NS300×10-C40 and
301 LS600×30-NS300×10-C40, are presented in Figs 8(a)–(c), while the load–carrying
302 contributions from the outer tube, concrete and inner tube, normalised by their corresponding

303 plastic loads (denoted $A_o\sigma_{0.2,o}$, $A_c f_c$ and $A_i\sigma_{0.2,i}$), are compared in Figs 8(d)–(f). It can be seen
304 that the slender stainless steel outer tube (LS600×5) was prone to local buckling and failed to
305 attain its yield load ($A_o\sigma_{0.2,o}$), while the more compact outer tubes (LS600×20 and LS600×30)
306 were able to exceed their yield loads and exhibit the pronounced strain hardening that
307 characterises stainless steel materials. The performance of the sandwiched concrete, in terms of
308 both strength and ductility, was also found to improve when a more compact outer tube was
309 used due to the greater confinement afforded to the concrete, as depicted in Fig 8(e).

310

311 Compared to the local slenderness of the outer tube, that of the inner tube was found to be less
312 influential on the ultimate response of the studied CFDST cross-sections. This can be seen in
313 Fig. 7, where, for a given d_o/t_o value, the difference in results between the CFDST stub columns
314 with varying d_i/t_i values is minimal. This is also evident in Fig. 9, where the normalised strength
315 N_u/N_{pl} can be seen to remain almost unaltered across the range of d_i/t_i ratios from 6 to 146.
316 Typical examples are shown in Fig. 10 for the examined CFDST stub columns with d_i/t_i ratios
317 of 26, 56 and 96. It can be seen that the performance of the outer tube and concrete appears not
318 to be greatly influenced by the compactness of the inner tube; in addition, despite the inner tube
319 failing by local buckling at a relatively low average axial strain for specimen LS600×3-
320 NS300×3-C40, the ultimate strength of the cross-section, which is dominated by the outer tube
321 and the concrete, is reached at a much later stage. Overall, it is concluded that the compactness
322 of the stainless steel outer tube has a substantial influence on the ultimate response of the
323 CFDST cross-sections, while the local slenderness of the carbon steel inner tube, which
324 represents only a relatively small contribution to the plastic resistance of the overall CFDST
325 cross-section, is less influential.

326

337 **3.3.2 Influence of concrete grade**

328 Three concrete grades were assessed in the parametric study, with nominal compressive
329 concrete strengths of 40, 80 and 120 MPa. The confined strength of the concrete is directly
330 linked to the cross-sectional compactness and is mainly governed by the local slenderness of
331 the outer tube. Comparisons of normalised strength (N_u/N_{pl}) were therefore made with respect
332 to the local slenderness of the outer tube (d_o/t_o), as shown in Fig. 11. It can be seen that the
333 lower concrete grades result in better normalised ultimate performance in the case of lower
334 outer tube slenderness values, revealing that lower concrete grades can benefit to a greater
335 extent from the confinement offered by the outer tube, provided that the tube is sufficiently
336 stocky.

337

338 **3.3.3 Influence of stainless steel grade**

339 Two stainless steel grades, lean duplex stainless steel (Grade 1.4062) and ferritic stainless steel
340 (Grade 1.4003), were examined in this study. The ultimate performance of CFDST cross-
341 sections utilising the two different grades of stainless steel for the outer tube are compared in
342 Fig. 12(a), revealing improved structural performance associated with the use of the lean duplex
343 grade, particularly in the case of the more compact outer tubes. This is attributed to the more
344 pronounced strain hardening and higher ductility of lean duplex stainless steel over ferritic
345 stainless steel, as displayed in Fig. 12(b).

346

347 **4. Evaluation of current international design codes**

348 **4.1 General**

349 The applicability of the European Code EN 1994-1-1 (EC4) [21], the Australian Standard AS
350 5100 [22] and the two American Specifications—AISC 360 [23] and ACI 318 [24] for
351 composite carbon steel members to the design of the studied CFDST cross-sections is appraised

352 in this section. Limitations on cross-sectional slenderness and material strengths specified in
353 the examined codes are summarised in Table 3. Note that although these code limitations are
354 exceeded for some of the tested [10] and modelled stub columns, comparisons and evaluations
355 are still presented to explore possible extension of the codes beyond their current range
356 applicability.

357

358 **4.2 European Code EN 1994-1-1 (EC4)**

359 The design expression for the axial compressive resistances of square or rectangular carbon
360 steel CFST cross-sections in EC4 [21] is a summation of the plastic resistance of the metal tubes
361 and concrete infill. Account is taken of the higher strength of the concrete infill as a result of
362 the confinement provided by the outer tube, by implementing a concrete coefficient of 1.0,
363 rather than 0.85. The analogous cross-section capacity (N_{EC4}) for a concrete-filled square or
364 rectangular CFDST cross-section in compression is thus given by Eq. (4).

$$365 \quad N_{EC4} = A_o \sigma_{0.2,o} + A_c f_c + A_i \sigma_{0.2,i} \quad (4)$$

366 A slenderness limit of $D_o/t_o \leq 52(235/f_y)^{0.5}$ for concrete-filled composite members is defined in
367 EC4 [21], beyond which the effects of local buckling need to be considered. In this study, this
368 slenderness limit is slightly modified to reflect the difference in Young's modulus between
369 stainless steel and carbon steel, thus: $D_o/t_o \leq 52\sqrt{(235/\sigma_{0.2,o})(E_o/210000)}$. For the CFDST cross-
370 sections exceeding this modified slenderness limit, the effective width formulation set out in
371 EN 1993-1-4 [35,36] for slender stainless steel internal plate elements, as given by Eq. (5), was
372 used for calculating the effective area of the outer tube, where ρ is the local buckling reduction
373 factor, and $\bar{\lambda}_p$ is the plate element slenderness and can be determined from Eq. (6), in which ν
374 is the Poisson's ratio, taken as 0.3, E_o is the Young's modulus of the outer tube, and k is the
375 buckling coefficient, taken equal to 4 for plates with simply supported boundary conditions in
376 pure compression [37,38].

377
$$\rho = \frac{0.772}{\bar{\lambda}_p} - \frac{0.079}{\bar{\lambda}_p^2} \quad (5)$$

378
$$\bar{\lambda}_p = \sqrt{\frac{\sigma_{0.2,o}}{\sigma_{cr}}} = \sqrt{\frac{12(1-\nu^2)\sigma_{0.2,o}}{k\pi^2 E_o}} (d_o/t_o) \quad (6)$$

379
380 **4.3 Australian Standard AS 5100**

381 The Australian Standard AS 5100 [22] adopts the same approach to obtain the axial
382 compressive design resistances as given in EC4 [21], but with a different slenderness limit and
383 effective width expression. A yield slenderness limit of 40 is specified for the flat faces of the
384 outer tube (λ_e) in AS 5100, where the local slenderness λ_e was also modified for stainless steel,
385 as given by $(d_o/t_o)(\sigma_{0.2,o}/250)^{0.5}$. For the design strengths of the test specimens and FE models
386 that exceed this limit, effective areas were again used in place of the gross areas to account for
387 local buckling. The effective width expression for cold-formed stainless steel tubular cross-
388 sections set out in AS/NZS 4673 [39] was adopted for the comparisons with the Australian
389 design provisions, as given by Eq. (7), where λ is a local slenderness, as given by Eq. (8), in
390 which F_n is the overall buckling stress of the column, equal to $\sigma_{0.2,o}$ due to the short length of
391 the studied stub columns, and k is again taken as 4 according to AS/NZS 4673 [39]. Hence, the
392 slenderness λ is essentially the same as that employed in EN 1993-1-4 [35], denoted $\bar{\lambda}_p$ and
393 defined by Eq. (5).

394
$$\rho = \frac{1 - 0.22 / \lambda}{\lambda} \quad (7)$$

395
$$\lambda = \left(\frac{1.052}{\sqrt{k}} \right) \frac{d_o}{t_o} \left(\sqrt{\frac{F_n}{E_o}} \right) \quad (8)$$

396

397 **4.4 American design provisions AISC 360 and ACI 318**

398 The AISC 360 compressive cross-section strength (N_{AISC}) for a square or rectangular concrete-
 399 filled column is presented as a function of the slenderness (compactness) of the flat faces of the
 400 steel section ($\lambda=d_o/t_o$), as determined from Eq. (9),

$$401 \quad N_{AISC} = \begin{cases} A_o\sigma_{0.2,o} + 0.85A_c f_c + A_i\sigma_{0.2,i} & (\lambda < \lambda_p) \\ P_p - \frac{P_p - P_y}{(\lambda_r - \lambda_p)^2} (\lambda - \lambda_p)^2 + A_i\sigma_{0.2,i} & (\lambda_p \leq \lambda < \lambda_y) \\ A_o f_{cr} + 0.7A_c f_c + A_i\sigma_{0.2,i} & (\lambda \geq \lambda_y) \end{cases} \quad (9)$$

402 where P_p and P_y are determined from Eq. (10) and (11) respectively, λ_p and λ_r correspond to
 403 the limits between compact/noncompact and noncompact/slender cross-sections, again
 404 modified for stainless steel herein, given by $2.26(E_o/\sigma_{0.2,o})^{0.5}$ and $3.00(E_o/\sigma_{0.2,o})^{0.5}$ respectively,
 405 and f_{cr} is the elastic critical local buckling stress of the outer tube, as given by Eq. (12). Note
 406 that the contribution from the inner tube in the resistance function is treated as an independent
 407 term, rather than a concrete dependent term as for reinforcing bars; further explanation has been
 408 provided in previous work by the authors [10–12].

$$409 \quad P_p = A_o\sigma_{0.2,o} + 0.85A_c f_c + A_i\sigma_{0.2,i} \quad (10)$$

$$410 \quad P_y = A_o\sigma_{0.2,o} + 0.7A_c f_c + A_i\sigma_{0.2,i} \quad (11)$$

$$411 \quad f_{cr} = \frac{9E_o}{(d_o/t_o)^2} \quad (12)$$

412 The American Concrete Institute design provisions for CFST cross-sections, as set out in ACI
 413 318 [24], are also assessed herein. The confinement afforded to the concrete from the steel tube
 414 is not explicitly considered in ACI 318. Hence, the cross-section resistance (N_{ACI}) is given by
 415 Eq. (13).

$$416 \quad N_{ACI} = A_o\sigma_{0.2,o} + 0.85A_c f_c + A_i\sigma_{0.2,i} \quad (13)$$

417 The gross area of the outer tube may be used in Eq. (13) provided that the tube thickness satisfies
 418 $t_o \geq D_o(\sigma_{0.2,o}/3E_o)^{0.5}$ [24]. For the design strengths of the test and FE specimens outside this

419 range, effective areas were again used in place of the gross areas to account for local buckling,
420 and the effective width expression for cold-formed stainless steel tubular cross-sections given
421 in the SEI/ASCE-8-02 [40] was utilised in the calculations. Note that SEI/ASCE-8-02 [40]
422 employs the same effective width formulation as AS/NZS 4673 [40], as given by Eq. (7).

423

424 **4.5 Assessment of current design methods**

425 In this section, the accuracy of the predicted cross-section compressive strengths from the
426 described design methods is evaluated by comparisons against the test and FE failure loads.
427 The mean test and FE to design code prediction ratios N_w/N_{code} , as presented in Table 4, are
428 respectively equal to 1.20, 1.17, 1.27, and 1.27 for EC4, AS 5100, AISC 360 and ACI 318, with
429 COVs of 0.108, 0.100, 0.131, and 0.086, revealing that the current design rules result in rather
430 conservative and scattered compressive strength predictions for the studied CFDST cross-
431 sections. The high level of conservatism and scatter is also evident in Figs 13–16, where the
432 ratios of N_w/N_{code} are plotted against the normalised cross-section slenderness (λ) of each
433 examined code, together with the corresponding normalised cross-section slenderness limits; a
434 summary of the normalised cross-section slenderness measures and limits is reported in Table
435 3. It can be seen that the predictions for the CFDST cross-sections falling within the slenderness
436 limits are unduly conservative, especially in the lower cross-section slenderness range, which
437 may be attributed to the lack of consideration for the substantial strain hardening that the
438 stainless steel outer tube exhibits and the higher degree of confinement afforded to the concrete
439 infill from the stockier outer tubes.

440

441 **5. Modifications to design rules**

442 **5.1 Modification to high strength concrete**

443 The results from the parametric analyses have revealed that the degree of influence of the
444 concrete strength on the compressive capacities of the studied CFDST stub columns differs
445 among the concrete grades, particularly for CFDST stub columns with compact outer tubes. It
446 is therefore suggested that this difference is reflected in the design formulations. It can also be
447 seen in Table 5 that the accuracy of the compressive strength predictions varies with concrete
448 grade for all the examined design codes. Specifically, the design predictions of CFDST cross-
449 sections with lower grade concrete were found to be more conservative than their counterparts
450 with higher grade concrete. This observation echoes the experimental results for the studied
451 CFDST cross-sections in [10], and also mirrors the findings for CFST cross-sections [14] and
452 other CFDST cross-sections [11,12]. To address this, it is proposed that the concrete strength
453 (f_c) in the design expressions is modified by multiplying by a reduction factor η , as specified in
454 EN 1992-1-1 [41] and given by Eq. (14), to account for the effective compressive strength of
455 high grade concrete (greater than 50 MPa). Note that the reduction factor η in EN 1992-1-1 [41]
456 only covers concrete strengths up to 90 MPa, beyond which a constant value of 0.8, as proposed
457 by Liew et al. [42], is employed herein.

$$458 \quad \eta = 1.0 - \frac{f_c - 50}{200} \quad (14)$$

459 The accuracy of the modified capacity predictions is assessed in Table 5, where the mean test
460 and FE to design code prediction ratios (N_u/N_{EC4*} , $N_u/N_{AS5100*}$, N_u/N_{AISC*} , and N_u/N_{ACI*}) and the
461 corresponding COVs for the three concrete grades are presented. The results from the
462 assessment reveal that with the inclusion of the reduction factor η , the modified capacity
463 predictions are more consistent and less scattered across the range of concrete grades from C40
464 to C120.

465

466 **5.2 Modification to design of steel tube**

467 The existing design codes were generally found to result in excessively conservative
468 compressive capacity predictions for the CFDST cross-sections exceeding the specified code
469 slenderness limits. This is can be primarily attributed to the neglect of the beneficial restraining
470 effect of the concrete on the local buckling of the stainless steel outer tubes. Unlike in hollow
471 SHS/RHS members, the local buckling failure mode of the outer tube in the examined CFDST
472 cross-sections features outward-only deformation of all four faces, rather than alternating
473 inward and outward deformations of adjacent faces. It has been shown that the elastic buckling
474 coefficient k [37,38] increases from 4 for conventional (two-way) local buckling of uniformly
475 compressed simply-supported plates to 10.67 for outward-only local buckling [43]. A modified
476 local buckling coefficient k equal to 10.67, rather than 4, has therefore been employed by the
477 authors [10,12] in previous studies to reflect the restraining effect of the concrete on the local
478 buckling of the stainless steel outer tubes. This approach is also assessed herein in the
479 implementation of the design rules in EC4, AS 5100 and ACI 318, taking the local buckling
480 coefficient k as 10.67 in calculating the plate slenderness and hence the effective areas of the
481 outer tubes. It is worth noting that due account of the outward-only buckling mode has already
482 been taken in AISC 360 [23] and reflected in the cross-section noncompact slenderness limit
483 [44,45], which is derived by factoring the corresponding limit for hollow steel cross-sections,
484 $1.40(E/F_y)^{0.5}$, by a value of $(10.67/4)^{0.5}$; further explanation is provided in previous work by the
485 authors [10].

486

487 Quantitative comparisons of the compressive capacities predicted by the modified EC4, AS
488 5100 and ACI 318 (N_{code^*}) incorporating the higher buckling coefficient k of 10.67, and the
489 corresponding predictions from the unmodified design rules with $k=4$, with test and FE ultimate
490 strengths are reported in Table 6 for the slender CFDST cross-sections that fall outside the

491 respective codified noncompact slenderness limits. The mean ratios of N_u/N_{code*} are all closer
492 to unity and less scattered than those for the case of $k=4$. The notably improved accuracy and
493 consistency is also evident in the graphical comparisons presented in Figs 13, 14 and 16,
494 respectively for the modified EC4, AS 5100 and ACI 318 predictions.

495

496 **5.3 Reliability analysis and discussion**

497 Statistical analyses were conducted to assess the reliability associated with the application of
498 the current and modified design rules to the examined CFDST cross-sections, according to the
499 procedures and requirements specified in EN 1990 [46]. In the present analyses, the mean to
500 nominal yield strength ratios $f_{y,mean}/f_{y,nom}$ were taken as 1.10 [47], 1.20 [47], and 1.16 [48], with
501 COVs of 0.030 [47], 0.045 [47] and 0.055 [48] for the lean duplex stainless steel, ferritic
502 stainless steel and the carbon steel, respectively. For the sandwiched concrete, the over-strength
503 ratio was determined from Eq. (15) [49],

$$504 \quad f_c = f_m - 1.64\delta \quad (15)$$

505 where f_m is the mean compressive concrete strength, and δ is the standard deviation, derived
506 from the measured COV values 0.019, 0.005 and 0.029 for C40, C80 and C120, respectively
507 [10]. The concrete over-strength ratios were therefore equal to 1.03, 1.01 and 1.05 for C40, C80
508 and C120, respectively, while the COV of the concrete strengths used in the reliability analysis
509 was conservatively taken as 0.180 [49] for all grades. The COVs of the geometric properties of
510 the stainless steel outer tube, concrete and carbon steel inner tube were taken as 0.05 [47], 0.01
511 [50] and 0.03 [48], respectively. Note that the partial factors for stainless steel, concrete and
512 carbon steel were taken as 1.10 [35], 1.50 [41] and 1.00 [51] in the assessment of the European
513 design provisions, while corresponding values of 1.11, 1.67 and 1.11 were used in the
514 assessment of the Australian design provisions, converted (inverted) from resistance factors of
515 0.9, 0.6 and 0.9 prescribed in AS 5100 [22] in the numerator rather than denominator. American

516 specifications consider the overall resistance factors, rather than individual partial factors in
517 composite design, with current recommended values in the numerator 0.75 and 0.65 for
518 concrete-filled tubular members, as specified in AISC 360 [23] and ACI 318 [24], respectively.
519 Therefore, the target partial safety factors for composite sections are equal to 1.0 for EC4 and
520 AS5100 design provisions since the individual target partial factors described above are already
521 included, and 1.33 and 1.54 for AISC 360 and ACI 318, respectively.

522

523 The key parameters and results from the Eurocode reliability analysis are summarised in Table
524 7, where $k_{d,n}$ is the design fractile factor, b is the average ratio of experimental and numerical
525 capacities to design model capacities [52], V_δ is the COV of the experimental and numerical
526 simulations relative to the resistance model, and γ_{M0} is the resulting partial safety factor for the
527 compressive strengths of the studied CFDST cross-sections. As can be seen from Table 7, the
528 required partial factors for the original and modified design rules are all close to or less than the
529 target values, and thus both the current and modified design rules are considered to satisfy the
530 reliability requirements of EN 1990 [46].

531

532 **6. Conclusions**

533 A comprehensive numerical modelling programme undertaken to examine the compressive
534 behaviour of CFDST cross-sections with lean duplex and ferritic stainless steel outer tubes is
535 reported in this paper. Finite element models have been established to replicate test results
536 reported in the literature, and utilised to acquire further FE data through parametric analyses.
537 The influence of key parameters on the ultimate response of the studied CFDST stub columns
538 was examined, including the local slendernesses of the outer and inner tubes, the concrete
539 strength and the stainless steel grade. The results of the parametric study generally revealed that
540 (i) the compactness of the stainless steel outer tube has a substantial influence on the ultimate

541 response of the CFDST cross-sections, while the local slenderness of the carbon steel inner tube
542 is less influential; (ii) the lower concrete grades can benefit to a greater extent from the
543 confinement offered by the outer tube; (iii) the use of lean duplex grade rather than ferritic
544 stainless steel for the outer tube results in superior CFDST compressive performance. Based on
545 the test and FE results, the applicability of the European Code EN 1994-1-1 (EC4) [21], the
546 Australian Standard AS 5100 [22] and the two American Specifications—AISC 360 [23] and
547 ACI 318 [24] for composite carbon steel members to the design of the studied CFDST cross-
548 sections was assessed. The assessment results generally indicated that the existing design rules
549 result in safe-sided, but unduly conservative (less so for the higher concrete grades) and rather
550 scattered capacity predictions.

551

552 Inaccuracies in the compressive resistance predictions stemmed principally from the lack of
553 consideration of strain hardening in the stainless steel outer tubes, insufficient allowance for
554 the restraining effect of the concrete against local buckling of the metal tubes and differences
555 in behaviour between high strength and normal strength concrete not being fully recognised.
556 Modifications to the current design provisions were therefore considered— a reduction factor
557 η to reflect the reduced relative effectiveness of using higher concrete grades and a higher
558 buckling coefficient k of 10.67 to consider the beneficial restraining effect of the concrete on
559 the local buckling of the stainless steel outer tubes. The modified design rules are shown to
560 yield greater accuracy and consistency, and their reliability was confirmed through statistical
561 analyses.

562

563 **Acknowledgements**

564 The authors are grateful to Mr. Cheuk Him Wong for his assistance in the experimental program
565 as part of his final year undergraduate research project at the University of Hong Kong. The

566 authors are grateful to STALA Tube Finland for supplying the test specimens. The research
567 work described in this paper was supported by a grant from the University of Hong Kong under
568 the seed funding program for basic research.

569

570 **References**

- 571 [1] T.M. Chan, L. Gardner, K.H. Law, Structural design of elliptical hollow sections: a review,
572 Proc. Inst. Civ. Eng. Struct. Build. 163(6) (2010) 391–402.
- 573 [2] L.-H. Han, W. Li, R. Bjorhovde, Developments and advanced applications of concrete-filled
574 steel tubular (CFST) structures: Members, J. Constr. Steel Res. 100 (2014) 211–228.
- 575 [3] S. Wei, S. Mau, C. Vipulanandan, S. Mantrala, Performance of new sandwich tube under axial
576 loading: experiment, ASCE J. Struct. Eng. 121(12) (1995) 1806–1814.
- 577 [4] K. Nakanishi, T. Kitada, H. Nakai, Experimental study on ultimate strength and ductility of
578 concrete filled steel columns under strong earthquake, J. Constr. Steel Res. 51(3) (1999) 297–
579 319.
- 580 [5] W. Li, Q.-X. Ren, L.-H. Han, X.-L. Zhao, Behaviour of tapered concrete-filled double skin steel
581 tubular (CFDST) stub columns, Thin-Walled Struct. 57 (2012) 37–48.
- 582 [6] X.-L. Zhao, L.-W. Tong, X.-Y. Wang, CFDST stub columns subjected to large deformation
583 axial loading, Eng. Struct. 32(3) (2010) 692–703.
- 584 [7] F. Zhou, B. Young, Compressive strengths of concrete-filled double-skin (circular hollow
585 section outer and square hollow section inner) aluminium tubular sections, Adv. Struct. Eng.
586 22(11) (2019) 2418–2434.
- 587 [8] L. Gardner, Stability and design of stainless steel structures – Review and outlook, Thin-Walled
588 Struct. 141 (2019) 208–216.
- 589 [9] L.-H. Han, Q.-X. Ren, W. Li, Tests on stub stainless steel–concrete–carbon steel double-skin
590 tubular (DST) columns, J. Constr. Steel Res. 67(3) (2011) 437–452.

- 591 [10] F. Wang, B. Young, L. Gardner, Experimental study of CFDST sections with stainless steel
592 SHS and RHS outer tubes under axial compression, *ASCE J. Struct. Eng.* 145(11) (2019)
593 04019139.
- 594 [11] F. Wang, B. Young, L. Gardner, Compressive testing and numerical modelling of concrete-
595 filled double skin CHS with austenitic stainless steel outer tubes, *Thin-Walled Struct.* 141
596 (2019) 345–359.
- 597 [12] F. Wang, B. Young, L. Gardner, CFDST sections with square stainless steel outer tubes under
598 axial compression: Experimental investigation, numerical modelling and design, *Eng. Struct.*
599 (2019) Under review.
- 600 [13] D. Lam, L. Gardner, Structural design of stainless steel concrete filled columns, *J. Constr. Steel*
601 *Res.* 64(11) (2008) 1275–1282.
- 602 [14] A. He, F. Wang, O. Zhao, Experimental and numerical studies of concrete-filled high-chromium
603 stainless steel tube (CFHSST) stub columns, *Thin-Walled Struct.* 144 (2019) 106273
- 604 [15] B. Uy, Z. Tao, L.-H. Han, Behaviour of short and slender concrete-filled stainless steel tubular
605 columns, *J. Constr. Steel Res.* 67(3) (2011) 360–378.
- 606 [16] B. Young, E. Ellobody, Experimental investigation of concrete-filled cold-formed high strength
607 stainless steel tube columns, *J. Constr. Steel Res.* 62(5) (2006) 484–492.
- 608 [17] Q.-H. Tan, L. Gardner, L.-H. Han, T.-Y. Song, Fire performance of steel reinforced concrete-
609 filled stainless steel tubular (CFSST) columns with square cross-sections, *Thin-Walled Struct.*
610 143 (2019) 106197.
- 611 [18] F. Wang, B. Young, L. Gardner, Experimental investigation of concrete-filled double skin
612 tubular stub columns with stainless steel outer tubes. *Proc. 8th Int. Conf. Steel Aluminium*
613 *Struct.*, Hong Kong, China, paper 118 (2016).
- 614 [19] M.F. Hassanein, O.F. Kharoob, Analysis of circular concrete-filled double skin tubular slender
615 columns with external stainless steel tubes, *Thin-Walled Struct.* 79 (2014) 23–37.
- 616 [20] F.-C. Wang, L.-H. Han, W. Li, Analytical behavior of CFDST stub columns with external
617 stainless steel tubes under axial compression, *Thin-Walled Struct.* 127 (2018) 756–768.

- 618 [21] European Committee for Standardisation (CEN), EN 1994-1-1:2004 Eurocode 4: Design of
619 Composite Steel and Concrete Structures – Part 1-1: General Rules and Rules for Buildings,
620 2004.
- 621 [22] Standards Australia, AS5100.6-2004 Bridge Design, Part 6: Steel and Composite Construction,
622 2004.
- 623 [23] American Institute of Steel Construction, ANSI/AISC 360-16 Specification for Structural Steel
624 Buildings, 2016.
- 625 [24] American Concrete Institute, ACI 318-14 Building Code Requirements for Structural Concrete
626 and Commentary, 2014.
- 627 [25] Karlsson Hibbitt, Sorensen, Inc. ABAQUS, ABAQUS/Standard User's Manual Volumes I–III
628 and ABAQUS CAE Manual. Version 6.12 Pawtucket (USA) 2012.
- 629 [26] A. He, Y. Liang, O. Zhao, Behaviour and residual compression resistances of circular high
630 strength concrete-filled stainless steel tube (HCFSSST) stub columns after exposure to fire, Eng.
631 Struct. 203 (2020) 109897.
- 632 [27] A. Espinos, L. Gardner, M. Romero, A. Hospitaler, Fire behaviour of concrete-filled elliptical
633 steel columns, Thin-Walled Struct. 49 (2) (2011) 239–255.
- 634 [28] Z. Tao, Z.B. Wang, Q. Yu, Finite element modelling of concrete-filled steel stub columns under
635 axial compression. J. Constr. Steel Res. 89 (2013) 121–131.
- 636 [29] A. He, O. Zhao, Experimental and numerical investigations of concrete-filled stainless steel
637 tube stub columns under axial partial compression, Journal of Constructional Steel Research
638 158 (2019) 405–416.
- 639 [30] R.B. Cruise, L. Gardner L. Strength enhancements induced during cold forming of stainless
640 steel sections, J. Constr. Steel Res. 64(11) (2008) 1310–1316.
- 641 [31] Wang F. Behaviour and design of concrete-filled double skin stainless steel members.
642 PhD thesis, Department of Civil engineering, the University of Hong Kong, Hong Kong,
643 China; 2018.

- 644 [32] B.W. Schafer, Z. Li, C.D. Moen, Computational modeling of cold-formed steel, *Thin-Walled*
645 *Struct.* 48(10-11) (2010) 752-762.
- 646 [33] P. Kyvelou, L. Gardner, D.A. Nethercot, Finite element modelling of composite cold-formed
647 steel flooring systems, *Eng. Struct.* 158 (2018) 28-42.
- 648 [34] G.B. dos Santos, L. Gardner, M. Kucukler, A method for the numerical derivation of plastic
649 collapse loads, *Thin-Walled Struct* 124 (2018) 258-277.
- 650 [35] European Committee for Standardisation (CEN), EN 1993-1-4:2006 Eurocode 3: Design of
651 Steel Structures – Part 1.4: General Rules –Supplementary Rules for Stainless Steels, 2006.
- 652 [36] L. Gardner, M. Theofanous, Discrete and continuous treatment of local buckling in stainless
653 steel elements, *J. Constr. Steel Res.* 64(11) (2008) 1207-1216.
- 654 [37] European Committee for Standardisation (CEN), EN 1993-1-5:2006 Eurocode 3: Design of
655 Steel Structures – Part 1-5: General rules - Plated structural elements, 2006.
- 656 [38] L. Gardner, A. Fieber, L. Macorini, Formulae for calculating elastic local buckling stresses of
657 full structural cross-sections, *Struct.* 17 (2019) 2-20.
- 658 [39] Standards Australia, AS/NZS 4673-2001 Cold-formed Stainless Steel Structures, 2001.
- 659 [40] American Society of Civil Engineers (ASCE), SEI/ASCE 8-02 Specification for the Design of
660 Cold-formed Stainless Steel Structural Members, 2002.
- 661 [41] European Committee for Standardization (CEN), EN 1992-1-1:2004 Eurocode 2: Design of
662 Concrete Structures-Part 1-1: General Rules and Rules for Buildings, 2004.
- 663 [42] J.Y.R. Liew, M. Xiong, D. Xiong, Design of Concrete Filled Tubular Beam-columns with High
664 Strength Steel and Concrete, *Struct.* 8 (2016) 213-226.
- 665 [43] B. Uy, M.A. Bradford, Elastic local buckling of steel plates in composite steel-concrete
666 members, *Eng. Struct.* 18(3) (1996) 193-200.
- 667 [44] Z. Lai, A.H. Varma, K. Zhang, Noncompact and slender rectangular CFT members:
668 Experimental database, analysis, design, *J. Constr. Steel Res.* 101 (2014) 455-468.
- 669 [45] R.T. Leon, D.K. Kim, J.F. Hajjar, Limit state response of composite columns and beam-columns
670 part 1: Formulation of design provisions for the 2005 AISC specification, *Eng. J. AISC* 44(4)
671 (2007) 341.

- 672 [46] EN 1990, Eurocode 0: basis of structural design. Brussels: European Committee for
673 Standardization (CEN), 2008.
- 674 [47] S. Afshan, P. Francis, N.R. Baddoo, L. Gardner, Reliability analysis of structural stainless steel
675 design provisions, *J. Constr. Steel Res.* 114 (2015) 293-304.
- 676 [48] M. Byfield, D. Nethercot, Material and geometric properties of structural steel for use in design,
677 *Struct. Eng.* 75 (1997) 363-367.
- 678 [49] Arya C. Design of structural elements. London: Spon Press; 2009.
- 679 [50] R. Lu, Y. Luo, J.P. Conte, Reliability evaluation of reinforced concrete beams, *Struct. Saf.* 14
680 (1994) 277-298.
- 681 [51] EN 1993-1-1, Eurocode 3: design of steel structures – Part 1. 1: general rules and rules for
682 buildings, Brussels: European Committee for Standardization (CEN), 2005.
- 683 [52] X. Meng, L. Gardner, A. J. Sadowski, J. M. Rotter, Elasto-plastic behaviour and design of semi-
684 compact circular hollow sections. *Thin-Walled Struct.* In press.

685
686

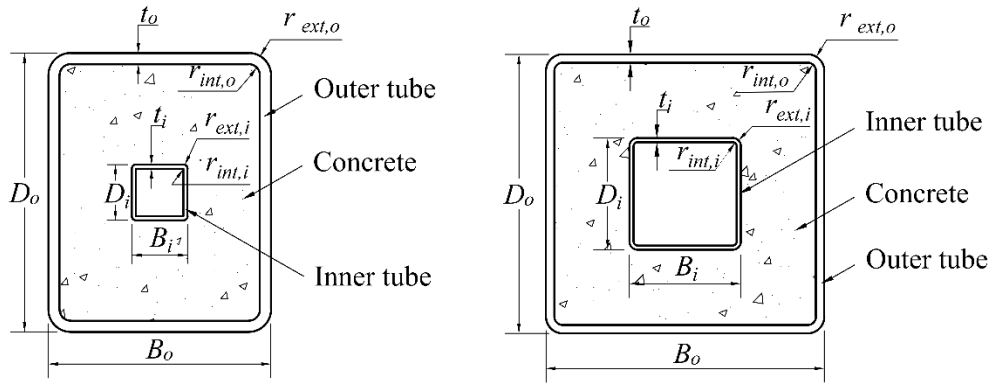
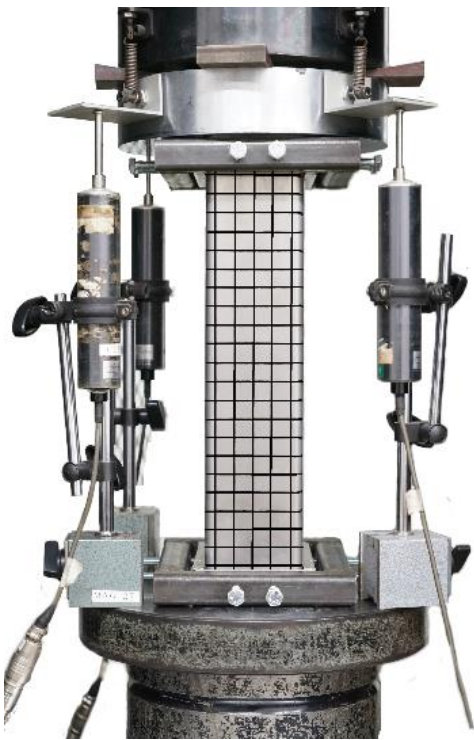
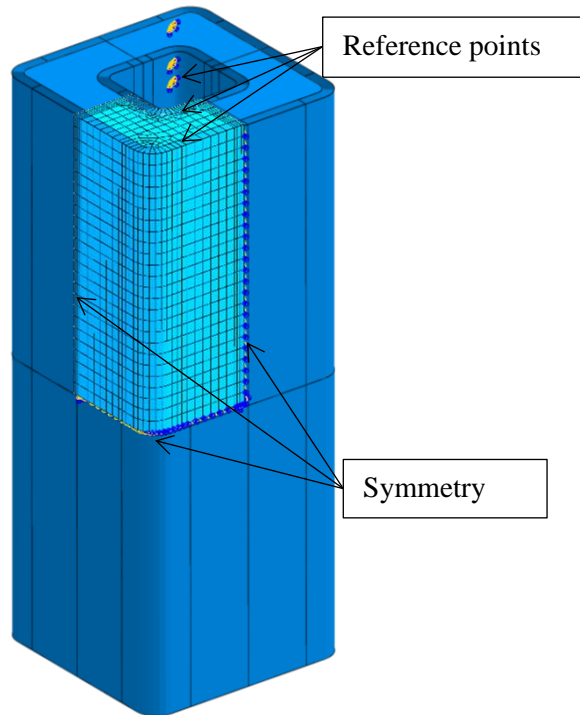


Fig. 1. Definition of symbols for CFDST specimens.

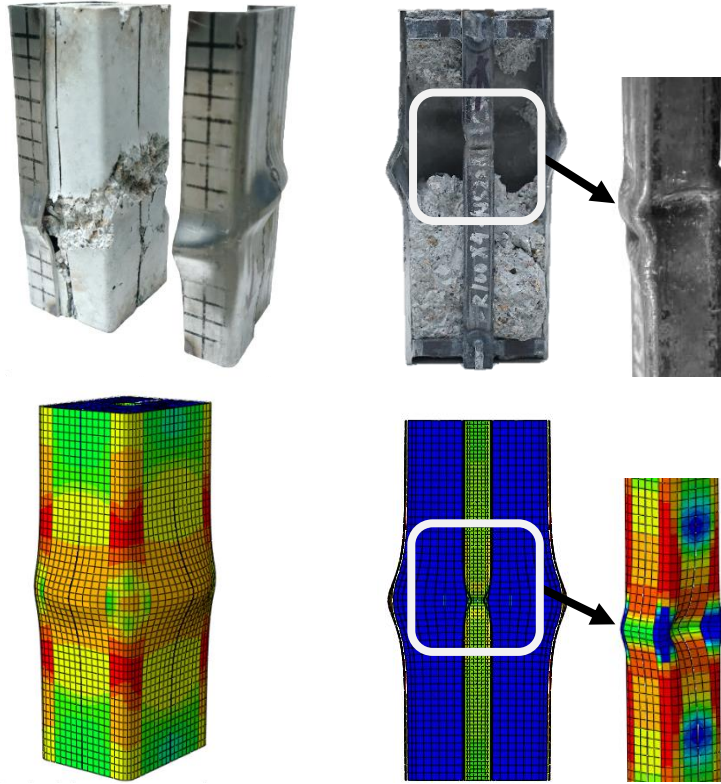


(a) Test setup.

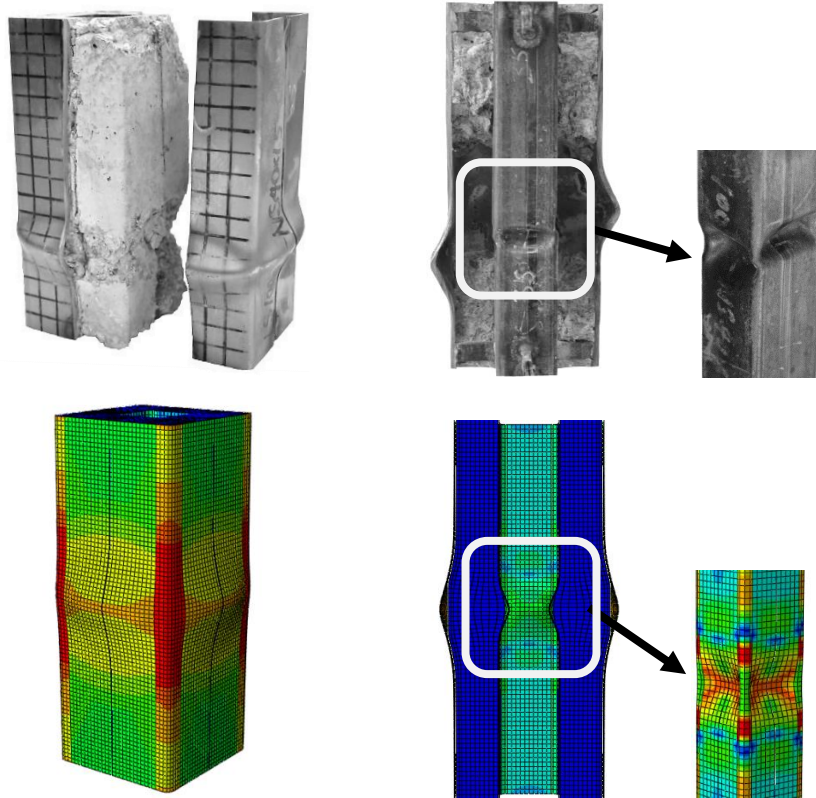


(b) FE model in ABAQUS.

Fig. 2. CFDST stub column (a) test setup and (b) FE model in ABAQUS.



(a) Outward local buckling of outer tube. (b) Inward and outward local buckling of inner tube.



(c) Outward local buckling of outer tube. (d) Inward local buckling of inner tube.

Fig. 3. Experimental and numerical failure modes of stub columns (FR100×4-NS20×1.5-C40 (a, b) LS100×3-NS40×1.5-C40 (c, d)).

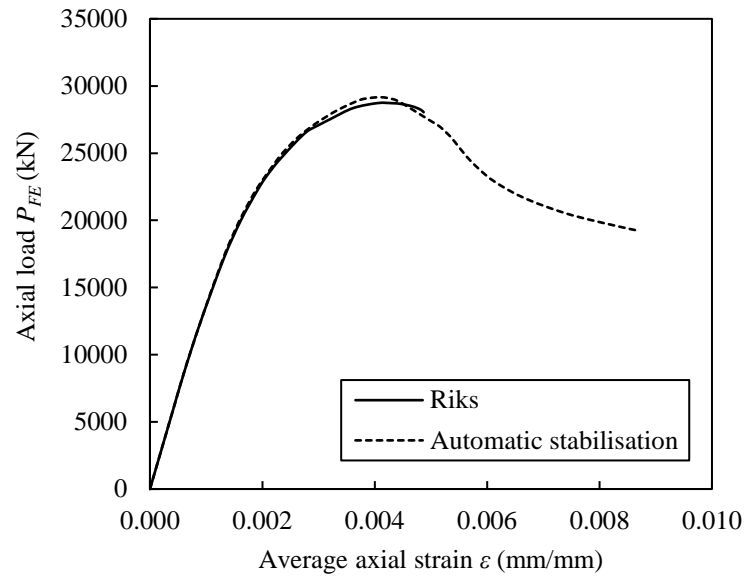


Fig. 4. Comparison of typical load–deformation responses generated from Riks and automatic stabilisation schemes.

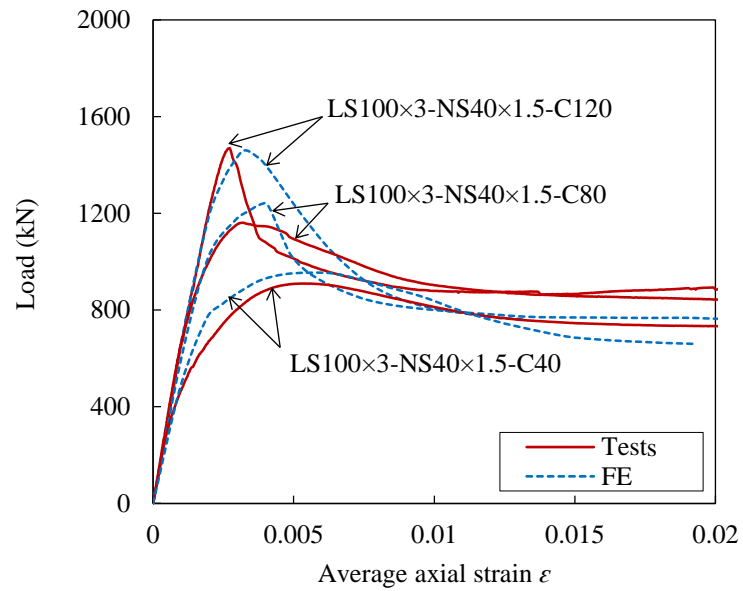


Fig. 5. Comparisons of test and FE load–average axial strain curves.

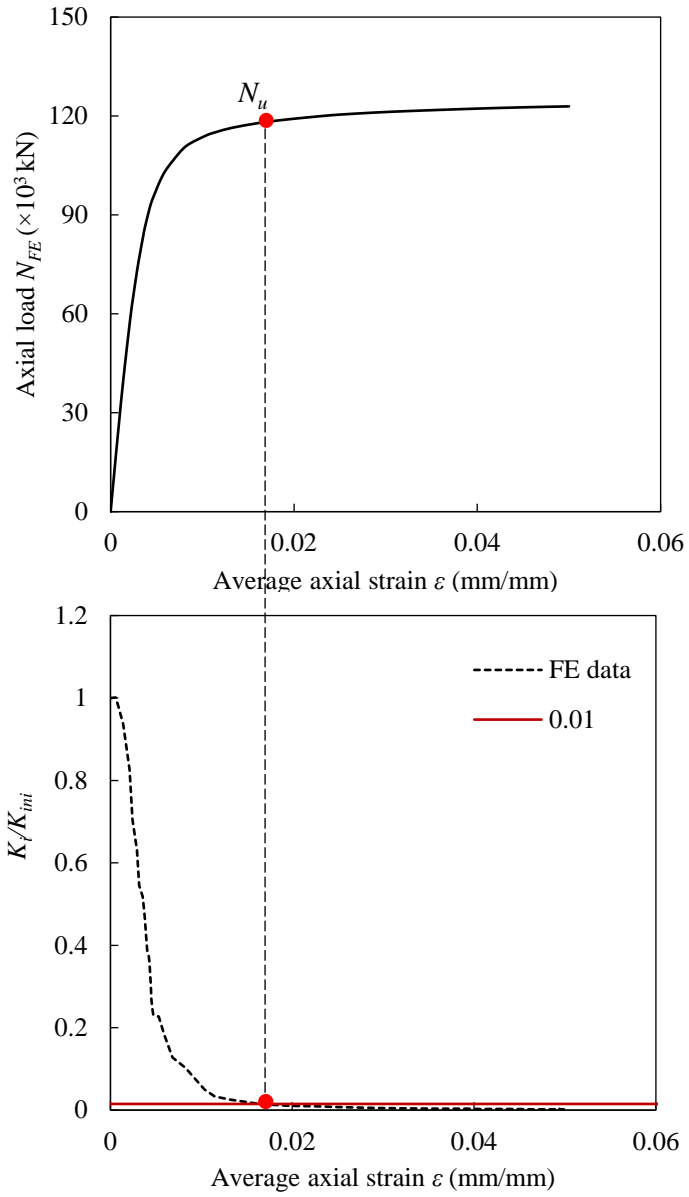


Fig. 6. Definition of ultimate axial compressive resistance when peak load was not attained in FE simulation.

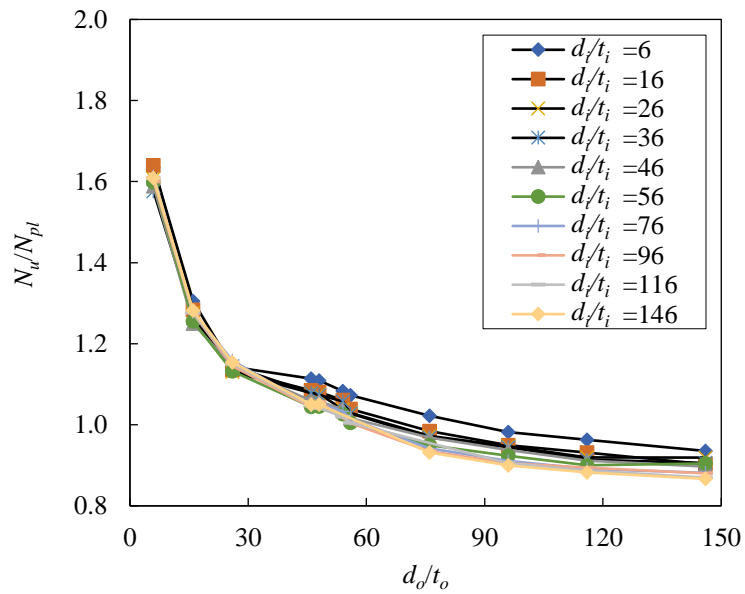
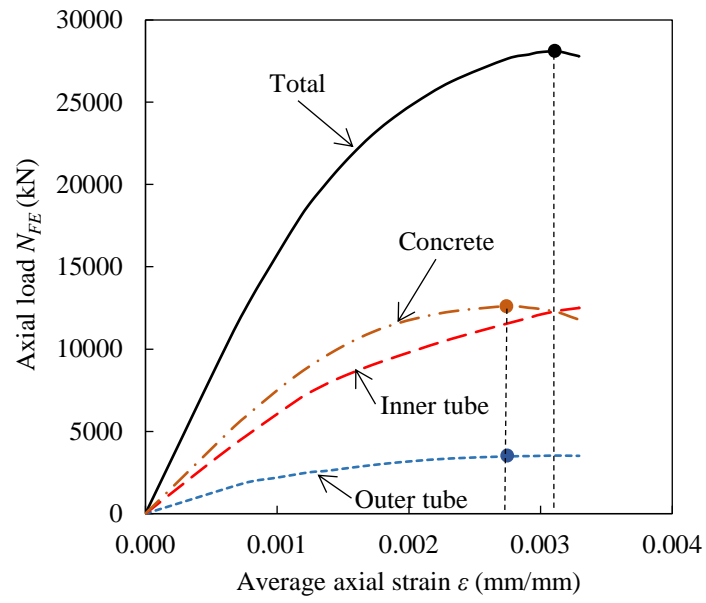
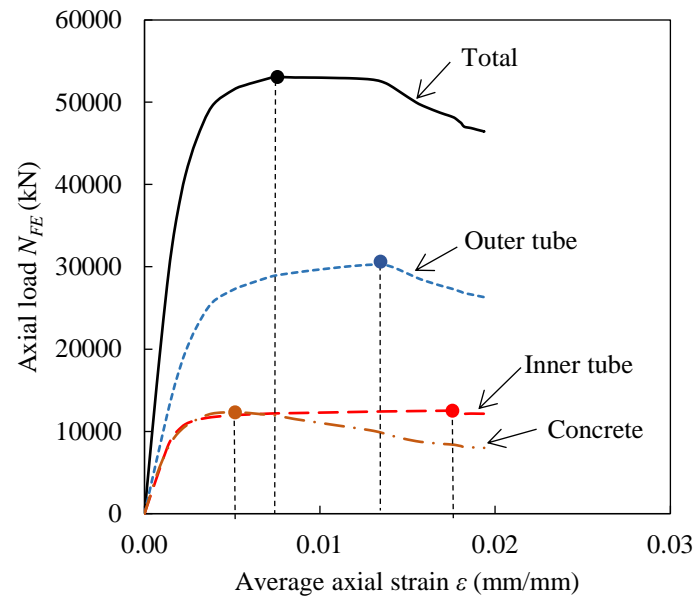


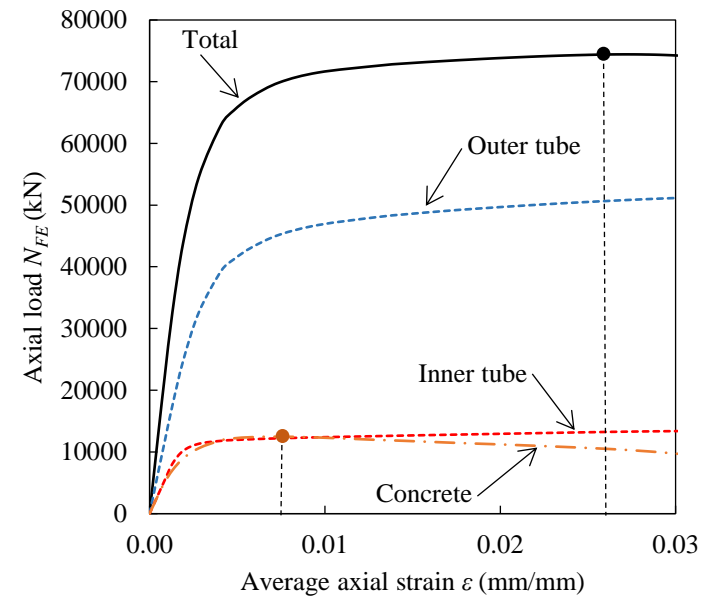
Fig. 7. Influence of outer tube slenderness on normalised resistance of studied CFDST cross-sections.



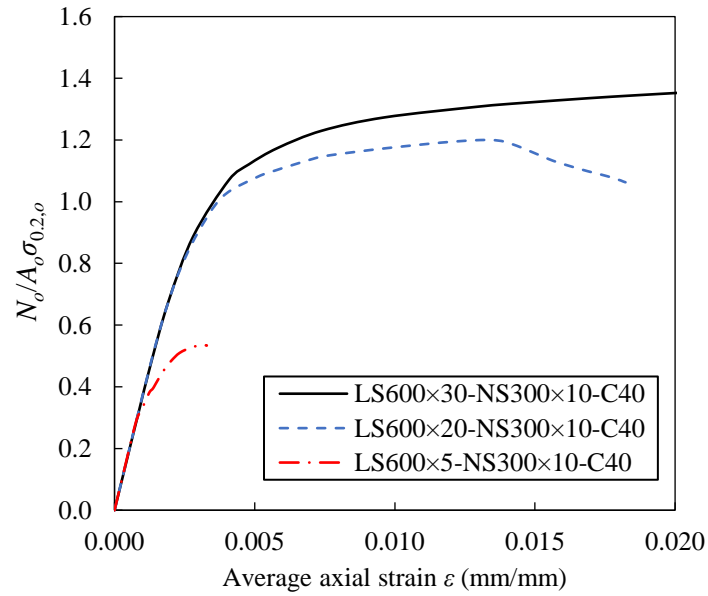
(a) Specimen LS600×5-NS300×10-C40.



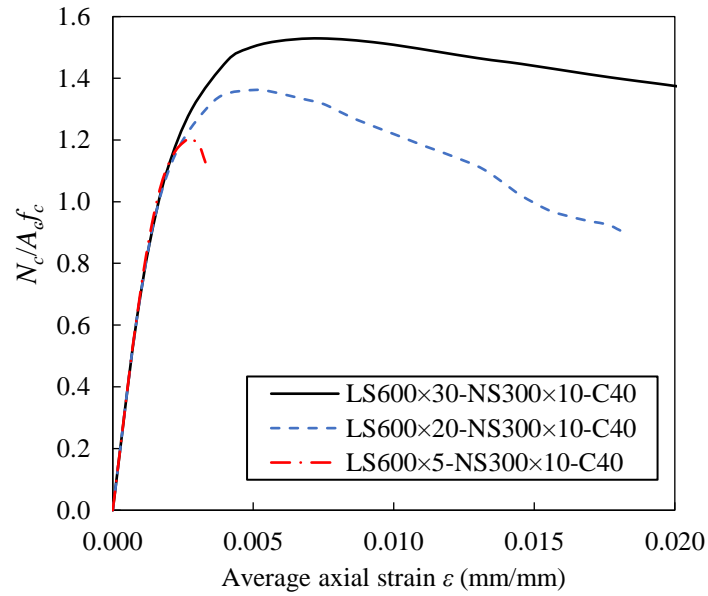
(b) Specimen LS600×20-NS300×10-C40.



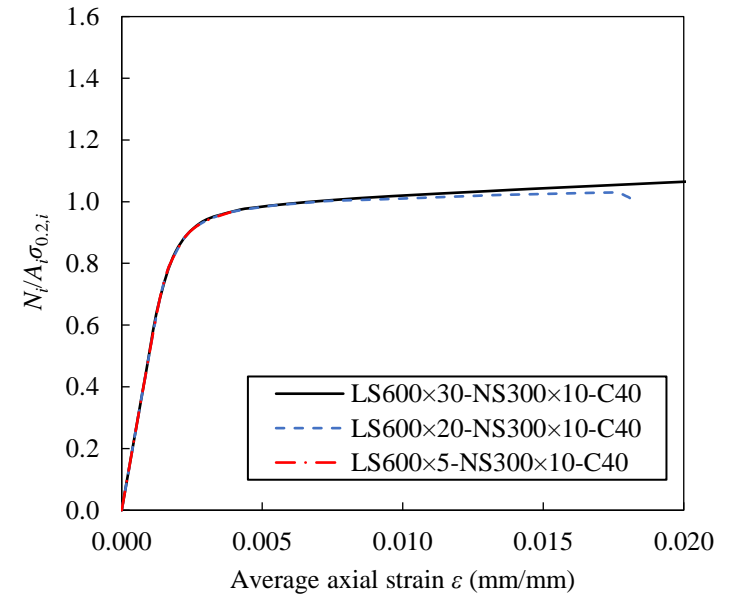
(c) Specimen LS600×30-NS300×10-C40.



(d) Performance of outer tubes.



(e) Performance of concrete.



(f) Performance of inner tubes.

Fig. 8. Comparisons of CFDST specimens with varying outer tube local slendernesses.

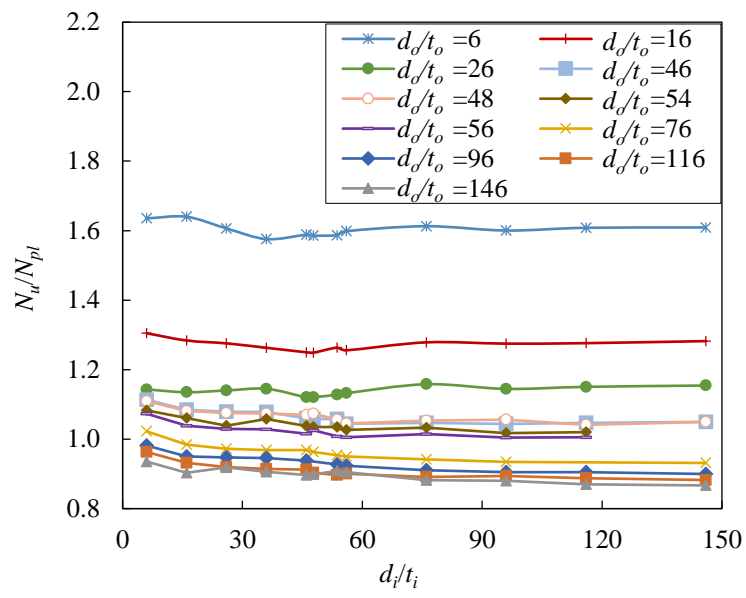


Fig. 9. Influence of inner tube slenderness on normalised load-carrying capacity of studied CFDST sections.

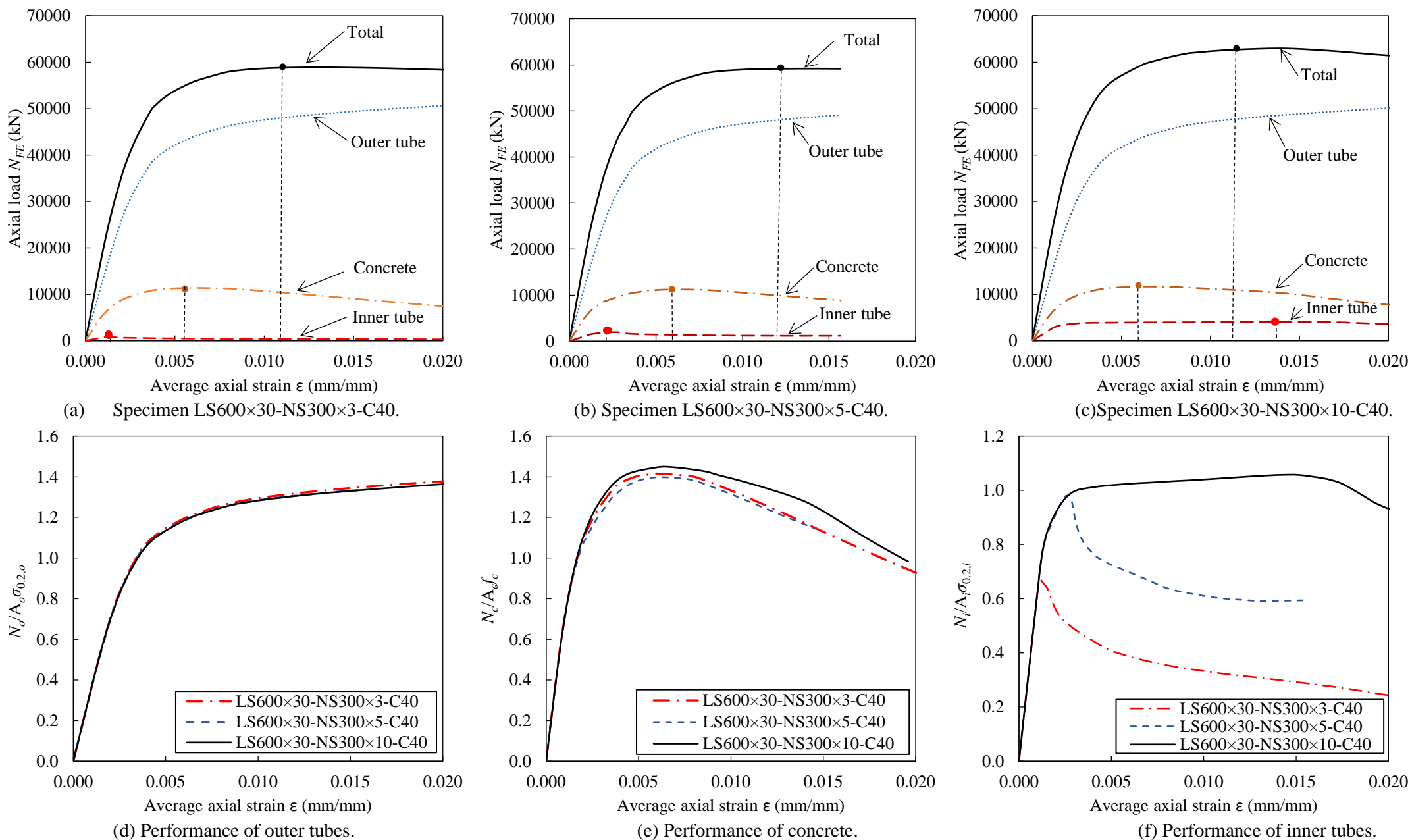


Fig. 10. Comparisons of CFDST specimens with varying inner tube local slendernesses.

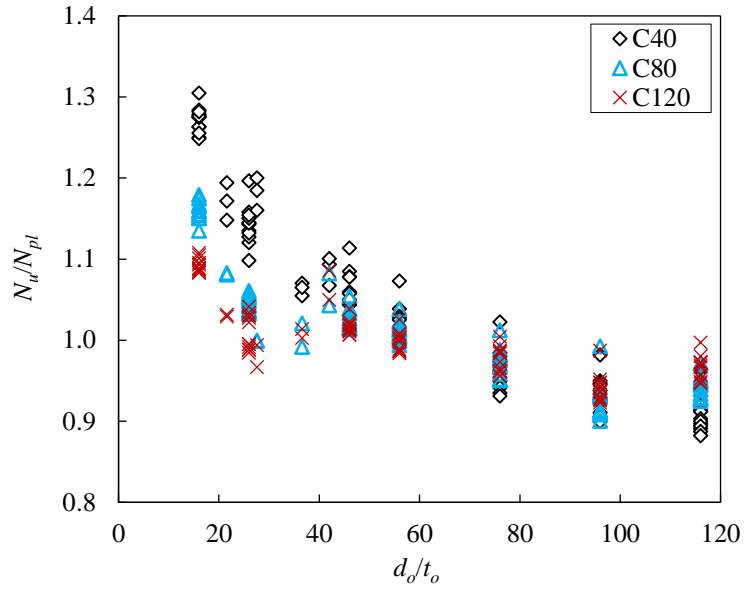
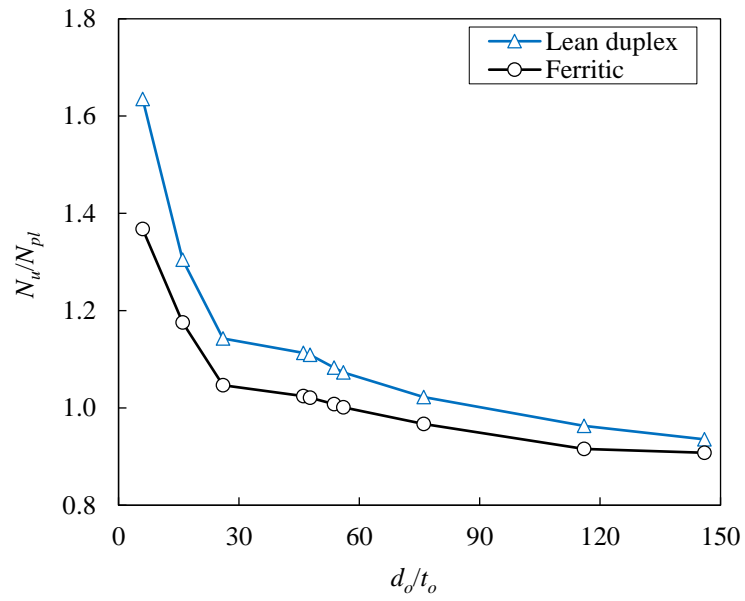
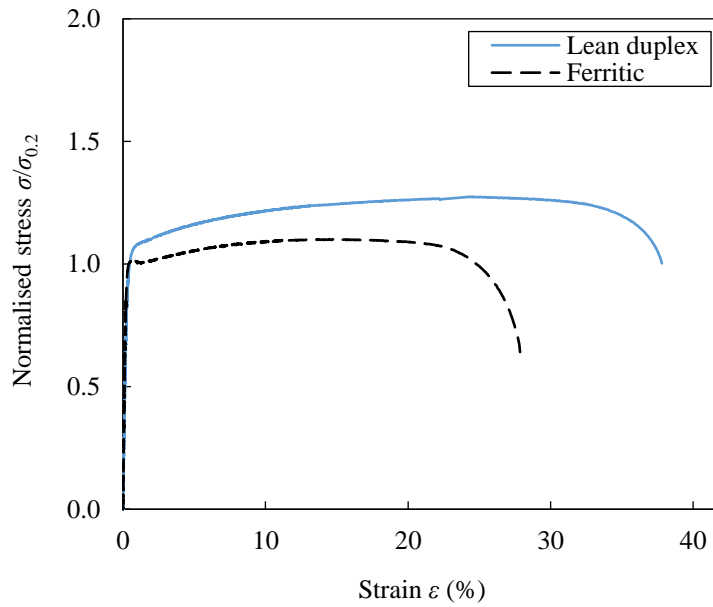


Fig. 11. Influence of concrete grade on normalised load-carrying capacity of studied CFDST sections.



(a) Comparisons of CFDST specimens of two different stainless steel grades.



(b) Normalised material properties of lean duplex and ferritic stainless steel.

Fig. 12. Influence of stainless steel grade on normalised load-carrying capacity of studied CFDST sections.

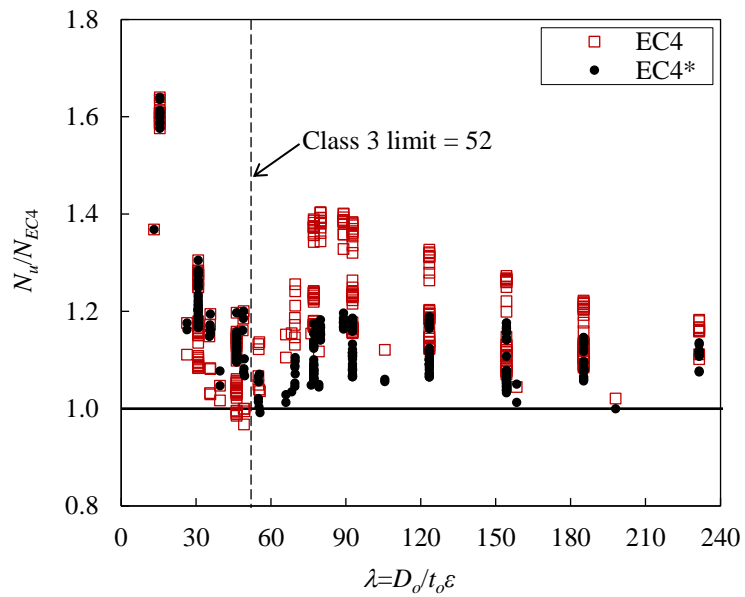


Fig. 13. Comparisons of test and FE results with strength predictions from EC4.

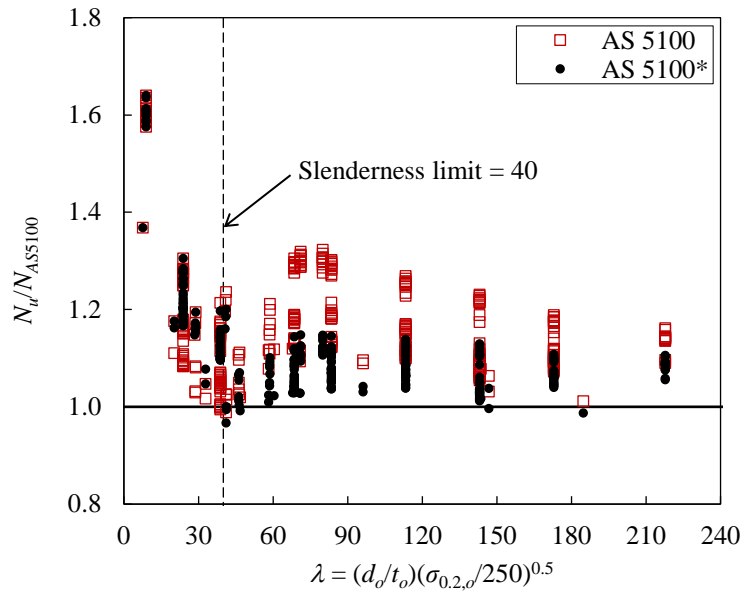


Fig. 14. Comparisons of test and FE results with strength predictions from AS 5100.

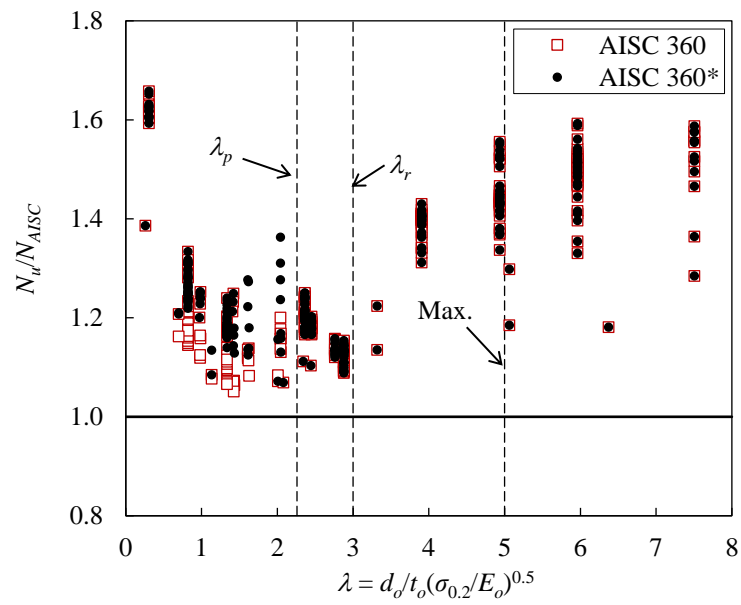


Fig. 15. Comparisons of test and FE results with strength predictions from AISC 360.

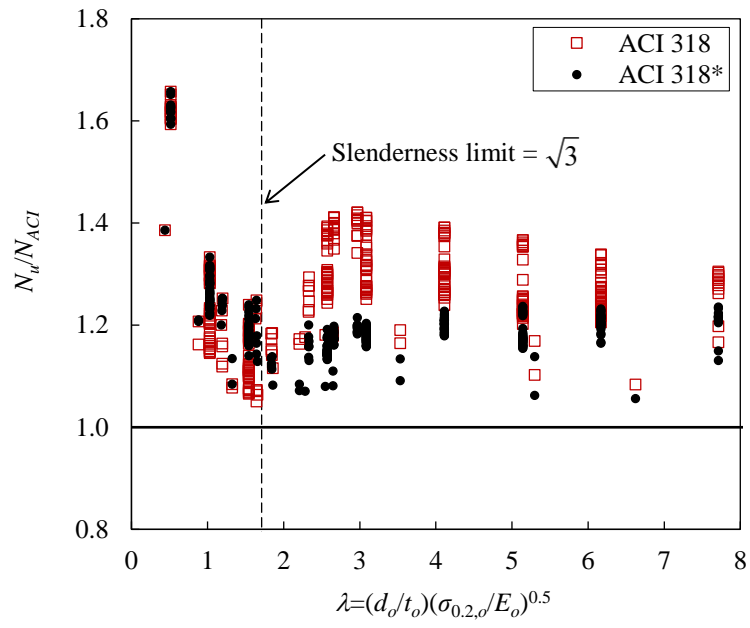


Fig. 16. Comparisons of test and FE results with strength predictions from ACI 318.

Table 1. Summary of experimental results on CFDST stub columns [10] and FE validation.

Specimen	D_o/t_o	D_i/t_i	$\sigma_{0.2,o}$ (MPa)	$\sigma_{0.2,i}$ (MPa)	f_c (MPa)	N_{exp} (kN)	N_{FE} (kN)	N_{FE}/N_{exp}
LR150×3-NS20×2.5-C40	48.6	7.7	475	468	41.8	1223	1313	1.07
LR150×3-NS20×2.5-C40R	48.6	7.7	475	468	41.8	1255	1313	1.05
LR150×3-NS20×2.5-C80	48.5	7.7	475	468	81.6	1681	1645	0.98
LR150×3-NS20×2.5-C120	48.4	7.7	475	468	115.9	1996	1963	0.98
LR150×3-NS20×1.5-C40	48.6	12.9	475	357	41.8	1216	1267	1.04
LR150×3-NS20×1.5-C80	48.5	13.2	475	357	81.6	1577	1594	1.01
LR150×3-NS20×1.5-C120	48.5	13.3	475	357	115.9	2019	1928	0.95
LS100×3-NS40×4-C40	31.8	10.4	556	404	41.8	1420	1354	0.95
LS100×3-NS40×4-C40R	31.7	10.4	556	404	41.8	1401	1354	0.97
LS100×3-NS40×4-C80	32.1	10.3	556	404	81.6	1464	1561	1.07
LS100×3-NS40×4-C120	31.9	10.4	556	404	115.9	1706	1774	1.04
LS100×3-NS40×1.5-C40	31.6	28.4	556	324	41.8	1209	1193	0.99
LS100×3-NS40×1.5-C80	31.8	28.1	556	324	81.6	1323	1401	1.06
LS100×3-NS40×1.5-C120	31.8	28.1	556	324	115.9	1516	1621	1.07
FR120×3-NS20×2.5-C40	41.9	7.7	401	468	41.8	910	954	1.05
FR120×3-NS20×2.5-C80	42.1	7.5	401	468	81.6	1161	1242	1.07
FR120×3-NS20×2.5-C120	41.7	7.7	401	468	115.9	1469	1460	0.99
FR120×3-NS20×1.5-C40	41.7	13.3	401	357	41.8	856	892	1.04
FR120×3-NS20×1.5-C40R	41.6	13.2	401	357	41.8	864	892	1.03
FR120×3-NS20×1.5-C80	41.7	13.1	401	357	81.6	1155	1196	1.04
FR120×3-NS20×1.5-C120	41.8	13.2	401	357	115.9	1409	1427	1.01
FR100×4-NS20×2.5-C40	26.1	13.1	439	468	41.8	1030	1036	1.01
FR100×4-NS20×2.5-C80	26.4	13.4	439	468	81.6	1235	1248	1.01
FR100×4-NS20×2.5-C120	26.4	13.4	439	468	115.9	1398	1427	1.02
FR100×4-NS20×1.5-C40	26.4	13.4	439	357	41.8	1015	990	0.98
FR100×4-NS20×1.5-C40R	26.3	13.1	439	357	41.8	999	990	0.99
FR100×4-NS20×1.5-C80	26.4	13.5	439	357	81.6	1191	1201	1.01
FR100×4-NS20×1.5-C120	26.3	13.1	439	357	115.9	1359	1386	1.02
Mean								1.02
COV								0.035
Max.								1.06
Min.								0.95

Table 2. Ranges of variation of parameters for the parametric study.

d_o/t_o	d_i/t_i	$\sigma_{0.2,o}$ (MPa)	$\sigma_{0.2,i}$ (MPa)	f_c (MPa)
6, 16, 26, 46, 48, 54, 56 76, 96, 116, 146	6, 16, 26, 36, 46 56, 76, 96, 116, 146	401, 556	404	40, 80, 120

Table 3. Code limits on cross-sectional slendernesses and material strengths.

Design codes	Limitations of cross-sectional slenderness		$\sigma_{0.2}$ (MPa)	f_c (MPa)
	Original	Normalised slenderness limits		
EN 1994-1-1	$D_o/t_o \leq 52 \sqrt{\frac{235}{\sigma_{0.2,o}} \frac{E_o}{210000}}$	$(D_o/t_o) \sqrt{\frac{210000}{E_o} \frac{\sigma_{0.2,o}}{235}} \leq 52$	235–460	20–50
AS 5100	$\lambda_e = \frac{d_o}{t_o} \sqrt{\frac{\sigma_{0.2,o}}{235}} \leq 40$	$\frac{d_o}{t_o} \sqrt{\frac{\sigma_{0.2,o}}{235}} \leq 40$	230–400	25–65
AISC 360	$\lambda_p = \frac{d_o}{t_o} \leq 2.26 \sqrt{\frac{E_o}{\sigma_{0.2,o}}}$	$\frac{d_o}{t_o} \sqrt{\frac{\sigma_{0.2,o}}{E_o}} \leq 2.26$	≤ 525	21–70
ACI 318	$t_o \geq D_o \sqrt{\frac{\sigma_{0.2,o}}{3E_o}}$	$(D_o/t_o) \sqrt{\frac{\sigma_{0.2,o}}{E_o}} \leq \sqrt{3}$	≤ 345	≥ 17.2

Table 4. Overall comparison of test and FE axial compressive strengths with predicted strengths.

No. of tests: 28	N_u/N_{EC4}	N_u/N_{EC4*}	N_u/N_{AS5100}	$N_u/N_{AS5100*}$	N_u/N_{AISC}	N_u/N_{AISC*}	N_u/N_{ACI}	N_u/N_{ACI*}
No. of FE modelling: 311								
Mean	1.20	1.14	1.17	1.12	1.27	1.29	1.27	1.21
COV	0.108	0.093	0.100	0.100	0.131	0.121	0.086	0.076

Table 5. Comparison of Test and FE strengths with design predictions for specimens falling within their respective codified slenderness limits.

f_c (MPa)		Ratio of test-to-predicted strengths							
		N_u/N_{EC4}	N_u/N_{EC4*}	N_u/N_{AS5100}	$N_u/N_{AS5100*}$	N_u/N_{AISC}	N_u/N_{AISC*}	N_u/N_{ACI}	N_u/N_{ACI*}
40	Mean	1.20	1.20	1.20	1.20	1.24	1.24	1.24	1.24
	COV	0.060	0.060	0.060	0.060	0.054	0.054	0.055	0.055
80	Mean	1.09	1.15	1.09	1.15	1.15	1.21	1.15	1.21
	COV	0.055	0.047	0.055	0.047	0.049	0.040	0.049	0.040
120	Mean	1.04	1.15	1.04	1.15	1.12	1.22	1.12	1.22
	COV	0.044	0.032	0.044	0.032	0.040	0.025	0.040	0.025

Table 6. Comparison of test and FE axial compressive strengths with design predictions for specimens exceeding their respective codified slenderness limits.

Parameters	Ratio of test-to-predicted strengths						
	N_u/N_{EC4}	N_u/N_{EC4*}	N_u/N_{AS5100}	$N_u/N_{AS5100*}$	N_u/N_{ACI}	N_u/N_{ACI*}	
Mean	1.21	1.10	1.17	1.07	1.29	1.18	
COV	0.083	0.042	0.069	0.036	0.053	0.029	

Table 7. Reliability analysis results calculated according to EN 1990 [46].

Design code	Sample type	Sample number	$k_{d,n}$	b	V_δ	Required value of γ_{MO}	Target value of γ_{MO}
EC4	Test+FE	28+311	3.119	1.20	0.111	1.00	1.00
EC4*	Test+FE	28+311	3.119	1.14	0.088	0.99	1.00
AS 5100	Test+FE	28+311	3.119	1.17	0.100	0.94	1.00
AS 5100*	Test+FE	28+311	3.119	1.12	0.095	0.98	1.00
AISC 360	Test+FE	28+311	3.119	1.27	0.114	1.15	1.33
AISC 360*	Test+FE	28+311	3.119	1.29	0.106	1.11	1.33
ACI 318	Test+FE	28+311	3.119	1.27	0.092	1.09	1.54
ACI 318*	Test+FE	28+311	3.119	1.21	0.073	1.10	1.54